HHS Public Access

Author manuscript

Nature. Author manuscript; available in PMC 2011 September 30.

Published in final edited form as:

Nature. 2011 March 31; 471(7340): 597–601. doi:10.1038/nature09797.

Habenular α5* nicotinic receptor signaling controls nicotine intake

Christie D. Fowler[1], **Qun Lu**[1], **Paul M. Johnson**[1], **Michael J. Marks**[2], and **Paul J. Kenny**[1]

[1]Laboratory for Behavioral and Molecular Neuroscience, Department of Molecular Therapeutics, The Scripps Research Institute – Scripps Florida, Jupiter, FL 33458, USA

[2]Institute of Behavioral Genetics, University of Colorado, Boulder, CO 80309, USA

Abstract

Genetic variation in *CHRNA5*, the gene encoding the α5 nicotinic acetylcholine receptor (nAChR) subunit, increases vulnerability to tobacco addiction and lung cancer, but underlying mechanisms are unknown. Here, we report dramatically increased nicotine consumption in mice with null mutation in *Chrna5*. This effect was `rescued' in knockout mice by re-expressing α5 subunits in medial habenula (MHb), and recapitulated in rats through α5 subunit knockdown in MHb. Remarkably, α5 subunit knockdown in MHb did not alter the rewarding effects of nicotine but abolished the inhibitory effects of higher nicotine doses on brain reward systems. The MHb extends projections almost exclusively to the interpeduncular nucleus (IPN). We found diminished IPN activation in response to nicotine in α5 knockout mice and disruption of IPN signaling increased nicotine intake in rats. Our findings suggest that nicotine activates the habenulo-interpeduncular pathway through α5-containing nAChRs, triggering an inhibitory motivational signal that acts to limit nicotine intake.

Tobacco smoking results in greater than 5 million deaths each year and accounts for almost 90% of all deaths from lung cancer1. Nicotine is the principal reinforcing component in tobacco smoke responsible for addiction2. Nicotine acts in the brain through the neuronal nicotinic acetylcholine receptors (nAChRs), which are ligand-gated ion channels consisting of five membrane-spanning subunits3. Twelve neuronal nAChR subunits have been identified, nine α subunits (α2–α10) and three β subunits (β2–β4)3. The predominant nAChR subtypes in mammalian brain that have been heavily implicated in regulating the addictive properties of nicotine are those containing α4 and β2 subunits (denoted α4β2* nAChRs)4,5,6,7,8. A major advance in our understanding of smoking behavior is the finding that allelic variation in the α5/α3/β4 nAChR subunit gene cluster located in chromosome

Correspondence and requests for materials should be addressed to P.J.K. (pjkenny@scripps.edu)..

Author Contributions C.D.F., Q.L., P.M.J. and M.J.M. performed all experiments; M.J.M. also provided essential reagents and assisted in manuscript editing; C.D.F. and P.J.K. designed the experiments, performed the statistical analyses and wrote the manuscript.

Supplementary /information Supplementary data is linked to the online version of the paper at www.nature.com/nature.

region 15q25 significantly increases risk of tobacco addiction9,10,11. In particular, polymorphisms in the α5 subunit gene (*CHRNA5*), which result in decreased function of the subunit, increase vulnerability to tobacco addiction12,13. Nevertheless, mechanisms through which α5* nAChRs may influence smoking behavior are unclear. Genetic variability in *CHRNA5* is also a major risk factor for lung cancer and chronic obstructive pulmonary disease (COPD) in smokers14,15,16, which may reflect higher levels of tobacco dependence in individuals carrying risk alleles and consequently greater exposure to carcinogens contained in tobacco smoke17, although the precise role of α5* nAChRs in lung cancer and COPD is unknown.

α5* nAChRs control nicotine intake

Here, we investigated the role of α5* nAChRs in the reinforcing properties of nicotine. We found that wildtype and knockout mice responded for intravenously self-administered nicotine infusions according to an inverted U-shaped dose-response curve, consistent with previous reports in humans18, non-human primates19, dogs20 and rats21. However, the knockout mice responded far more vigorously than wildtype mice for nicotine infusions, especially when higher unit doses were available (Fig. 1a); see Ref.22. Increased responding for nicotine in knockout mice was not secondary to alterations in operant performance or the motivational salience of reward-paired conditioned stimuli (Supplementary Fig. 1). When we calculated total amounts of nicotine consumed at each dose available for self-administration, we found that wildtype mice titrated their responding to consume ~1.5 mg kg^{-1} per session (Fig. 1b); which achieves plasma concentrations of nicotine comparable to those detected in humans after 5 h of smoking their preferred brand of cigarette23,24. In contrast, knockout mice did not titrate their responding and consumed greater amounts of nicotine as the dose increased (Fig. 1b). Knockout mice also had greater motivation to seek and obtain nicotine when tested under a progressive ratio schedule of reinforcement, an effect most apparent again at high doses (Supplementary Fig. 2). Enhanced responding for nicotine as the unit dose increases is thought to reflect an intensification of the reinforcing properties of the drug, thereby motivating higher levels of intake25. Diminished responding as the dose increases reflects greater restraint over intake to avoid the increasingly aversive effects of higher drug doses18,25 or more rapid development of drug satiation25,26. Our findings therefore suggest that deletion of α5 nAChR subunits has a dissociable effect on the motivational drives that control nicotine intake. The stimulatory effects of nicotine on brain reinforcement systems (i.e., ascending portion of dose-response curve) are unaltered by α5 subunit knockout, since the wildtype and knockout mice responded for nicotine at a similar maximal rate. Instead, deficient α5* nAChR signaling appears to attenuate the negative effects of nicotine that limit its intake (i.e., descending portion of dose-response curve). These findings are highly consistent with the increased vulnerability to tobacco addiction in human smokers carrying *CHRNA5* risk alleles that result in less functional α5* nAChRs12,13.

Habenular α5* nAChRs control nicotine intake

The α5 nAChR subunit has a restricted distribution profile in the brain, with dense expression in the habenulo-interpeduncular pathway, deep layers of the cortex and

hippocampus, and lower expression in the ventral tegmental area (VTA) and substantia nigra27. The medial habenula (MHb) projects almost exclusively to the interpeduncular nucleus (IPN) via the fasciculus retroflexus28. Functional α5* nAChRs are expressed on MHb afferents to the IPN29, and high but not low nicotine doses activate the habenulo-interpeduncular tract, as measured by an increased local glucose utilization in rats30. The habenulo-interpeduncular tract regulates avoidance of noxious substances31 and regulates somatic aspects of nicotine withdrawal32. However, little is known of its role in drug-taking behavior33. Intriguingly, the lateral habenula (LHb) has an inhibitory influence on VTA dopamine neurons34, is activated by aversive stimuli or omission of anticipated reward, and is considered a source of negative motivational signals in the brain34. We therefore hypothesized that nicotine-induced stimulation of α5* nAChRs in the habenulo-interpeduncular pathway triggers an inhibitory motivational signal that limits consumption of the drug. In knockout and wildtype mice that received injections of a control lentivirus expressing green-fluorescent protein (GFP; Lenti-Control) into the MHb, we again found that knockout mice self-administered far greater amounts of nicotine when a high unit dose was available (Fig. 2a), replicating the above findings. However, nicotine intake was indistinguishable in knockout versus wildtype mice after injection of a lentivirus vector (Lenti-CHRNA5) into the MHb to rescue α5 nAChR subunits in the habenulo-interpeduncular tract (Fig. 2b; Supplementary Fig. 3). GFP immunostaining to confirm MHb delivery of virus was carried out for the majority of the mice. Responding for nicotine (0, 0.1 and 0.4 mg kg^{-1} per infusion) in the subset of Lenti-CHRNA5-treated used for immunostaining 3.6 ± 0.83, 8.8 ± 1.4 and 4.86 ± 1.0, respectively, for wildtypes and 4.53 ± 0.85, 7.72 ± 0.68 and 4.53 ± 1.4, respectively, for knockouts. GFP immunostaining confirmed that virus-infected cells were detected almost exclusively in the habenulo-interpeduncular tract of Lenti-CHRNA5 knockout mice, with little detectable staining in other brain areas that could potentially impact self-administration behavior (Fig. 2c,d; Supplementary Fig. 4). The remaining mice not used for immunostaining were used to verify that the Lenti-CHRNA5 virus was function. Real-time PCR verified that α5 subunit mRNA was detectable only in habenula (Supplementary Fig. 5) and IPN (Supplementary Fig. 6) of the Lenti-CHRNA5-treated knockout mice, suggesting that α5 nAChR subunit mRNA is transported from the MHb along the fasciculus retroflexus and into the IPN. Wildtype mice treated with the Lenti-CHRNA5 vector did not demonstrate increased α5 subunit mRNA above baseline levels in the habenula (Supplementary Fig. 5), suggesting that strict regulatory mechanisms control α5* nAChR expression in the MHb-IPN pathway.

Using radiolabeled rubidium ($86Rb^+$) efflux as a functional measure of nAChR signaling, we found that acetylcholine-evoked $86Rb^+$ efflux was dramatically attenuated in synaptosomes prepared from the habenula and IPN, but not the cortex or hippocampus, of a separate cohort of knockout versus wildtype mice (Supplementary Fig. 7). Consistent with a recent report, $86Rb^+$ efflux was also attenuated in synaptosomes from the thalamus of knockout mice35 (Supplementary Fig. 7). Injections of lenti-CHRNA5 into MHb attenuated the deficits in $86Rb^+$ efflux in IPN, but not in MHb or thalamus, of knockout mice (Supplementary Fig. 8). These findings demonstrate that α5* nAChRs play a critical role in regulating nAChR transmission in the habenulo-interpeduncular tract, and confirm that the Lenti-CHRNA5 vector rescues not only expression, but also function, of α5* nAChRs in the

habenulo-interpeduncular pathway. These data also reveal three additional insights: First, α5 subunits produced in MHb are predominately incorporated into α5* nAChRs expressed presynaptically on afferents to IPN. Second, injections of the Lenti-CHRNA5 vector into MHb rescued local α5 subunit mRNA expression, but not deficits in MHb $86Rb^+$ efflux. This suggests that nAChR signaling in MHb may be derived from α5* nAChRs located presynaptically on afferent inputs from brain sites not infected by the virus. Third, whilst the Lenti-CHRNA5 vector attenuated the deficits in nAChR signaling detected in IPN of knockout mice, this rescue was only partial (Fig. 2e). Hence, postsynaptically localized α5* nAChRs on IPN neurons, or perhaps presynaptic α5* nAChRs on afferent inputs that originate from brain sites other than the MHb, also play a major role in nAChR transmission in the IPN.

Next, we developed and validated a lentivirus vector to deliver a short-hairpin interfering RNA against the α5 nAChR subunit (Lenti-α5-shRNA; Supplementary Fig. 9). We then microinjected the Lenti-α5-shRNA vector into the MHb of rats to knockdown habenulo-interpeduncular α5* nAChRs (Supplementary Fig. 10). As expected, Lenti-Control rats responded for nicotine according to an inverted U-shaped dose-response curve (Fig. 3a). There was a dramatic increase in nicotine consumption across the dose-response curve in the Lenti-α-shRNA rats that was most apparent at high unit doses (Fig. 3a). When total nicotine intake at each dose was calculated, we found that Lenti-Control rats titrated their responding to consume ~0.75–1 mg kg^{-1} nicotine per session (Supplementary Fig. 10). In contrast, knockdown rats showed little evidence of titration and continued to increase their consumption as the unit dose increased. We obtained similar effects on nicotine intake using a second lentivirus vector that expressed an shRNA targeting a different portion of α5 subunit mRNA (Supplementary Fig. 11). Overall, these findings in rats recapitulate those in the α5 knockout mice and confirm that α5* nAChRs in the habenulo-interpeduncular pathway regulate levels of nicotine intake across species.

α5* nAChRs inhibit brain reward function

Next, we examined the effects of nicotine on brain-stimulation reward (BSR) thresholds in rats following knockdown of α5* nAChRs in the habenulo-interpeduncular pathway. In the BSR procedure, rats respond vigorously to obtain rewarding electrical self-stimulation via an intracranial stimulating electrode, with the minimal stimulation intensity that maintains self-stimulation behavior termed the reward threshold. Low doses of nicotine (~0.25 mg kg^{-1}) that condition a place preference in rats also lower BSR thresholds36, reflecting drug-induced enhancement of brain reward activity. Conversely, higher doses of nicotine (≥1 mg kg^{-1}) that condition a place aversion can elevate BSR thresholds in rats37. Importantly, rats regulate their pattern of nicotine self-administration behavior at a level that achieves maximal lowering of BSR thresholds36, suggesting that obtaining the stimulatory effects of nicotine on brain reward circuits, whilst avoiding its negative effects, determines the amounts of nicotine consumed by rats. We found that low doses of nicotine (0.125–0.25 mg kg^{-1}; free-base; SC) lowered BSR thresholds by a similar magnitude in the Lenti-Control and Lenti-α5-shRNA rats (Fig. 3b). However, as the dose of nicotine was increased (1–1.5 mg kg^{-1}; free-base; SC), BSR thresholds were elevated above baseline in Lenti-Control rats, but continued to be lowered below baseline levels in Lenti-α5-shRNA rats (Fig. 3b). These

data demonstrate that the stimulatory effects of nicotine on brain reward systems, which likely provide a crucial source of reinforcement that maintains the tobacco smoking habit38, are unaltered by deficits in α5* nAChRs in the MHb-IPN pathway. Instead, the inhibitory effects of higher nicotine doses on the activity of reward circuitries, which likely determine the amounts of nicotine that can be consumed, are greatly attenuated by knockdown of α5* nAChRs in this pathway.

Habenular α5* nAChRs regulate IPN activation

The $86Rb^+$ efflux data above suggest that α5 subunits transcribed in the MHb are incorporated into presynaptic α5* nAChRs in the IPN where they may regulate neurotransmitter release. Acetylcholine and glutamate are the major neurotransmitters produced by MHb neurons innervating the IPN39, and presynaptic α5* nAChRs are thought to regulate glutamate but not acetylcholine release in IPN29,40,41 Interestingly, glutamatergic transmission at the MHb-IPN synapse is increased in response to nicotine concentrations likely achieved in the brains of smokers42. We therefore hypothesized that deficient α5* nAChR signaling in the habenulo-interpeduncular tract may decrease nicotine-evoked glutamatergic transmission in the IPN and thereby attenuate a negative motivational signal that limits its intake. Consistent with this hypothesis, an aversive higher dose of nicotine (1.5 mg kg^{-1})43, but not a rewarding lower dose (0.5 mg kg^{-1})43, robustly activated the IPN in wildtype mice, reflected in increased Fos immunoreactivity (Fig. 4a,b). This effect of the high nicotine dose was almost completely abolished in the knockout mice. Wildtype and α5 knockout mice displayed similar Fos immunoreactivity in the ventromedial hypothalamus (Supplementary Fig. 12), a region in which Fos induction is highly stress responsive44, suggesting that altered stress responses in knockout mice did not account for this effect. Nicotine-induced increases in Fos immunoreactivity in the VTA, which controls the reinforcing effects of nicotine, were similar in wildtype and α5 knockout mice (Supplementary Fig. 13). Nevertheless, there was a non-statistically significant trend toward lower VTA Fos immunoreactivity in the knockout mice in response to the high nicotine dose. Considering that the VTA can also regulate aversive responses to nicotine45, it is possible that α5* nAChRs in VTA may differentially regulate activation of this structure in response to aversive but not rewarding doses of nicotine. Taken together, these findings are consistent with our behavioral data in which the reinforcing effects of nicotine, likely involving VTA activation, are substantially conserved in the knockout mice. However, recruitment of an aversive/satiety pathway by nicotine overconsumption, likely involving habenular-driven activation of IPN, is diminished in animals with deficient α5* nAChR signaling.

Habenular-IPN activity limits nicotine intake

We next examined the effects of reversible inactivation of the habenulo-interpeduncular tract on nicotine self-administration behavior in rats, accomplished by direct microinjection of lidocaine into targeted brain sites. Lidocaine-induced inactivation of the IPN increased responding for nicotine (0.03 mg kg^{-1} per infusion) (Fig. 5a; Supplementary Fig. 14), further supporting a role for nicotine-induced activation of the IPN in restricting nicotine intake. Conversely, inactivation of the VTA profoundly decreased nicotine intake (0.03 mg

kg^{-1} per infusion) (Supplementary Fig. 15, 16). Inactivation of the MHb increased nicotine intake similar to IPN inactivation (Fig. 5b), but this effect was only detected when rats self-administered a higher (0.12 mg kg^{-1} per infusion) unit dose of nicotine (Supplementary Figs. 17, 18). This effect is consistent with habenular-mediated activation of the IPN preferentially occurring when higher nicotine doses are consumed. Next, we investigated the role of glutamate-mediated transmission in these brain sites in regulating nicotine intake. Microinjection of the competitive *N*-methy-D-aspartate (NMDA) glutamate receptor antagonist LY23595946 into the IPN dose-dependently increased nicotine self-administration (Fig. 5c). LY235959 infused into MHb also increased nicotine intake at the higher unit dose of nicotine, whereas infusion into VTA decreased nicotine intake (Fig, 5d; Supplementary Fig. 16). Taken together, these data support a conceptual framework in which high levels of nicotine intake stimulate the habenulo-interpeduncular tract through α5* nAChRs and thereby enhance NMDA receptor-mediated glutamatergic transmission in the IPN. This nicotine-induced enhancement of IPN activity relays an inhibitory motivational signal that limits further drug intake. Deficient α5* nAChR signaling diminishes the magnitude of this inhibitory motivational signal, permitting larger amounts of nicotine to be consumed (Supplementary Fig. 19).

Our findings reveal the habenulo-interpeduncular pathway as a key neurocircuit controlling nicotine intake. This circuit acts in a manner opposite to the mesoaccumbens `positive reward' pathway and instead transmits an inhibitory motivational signal that limits nicotine intake. There are reciprocal projections between the MHb and portions of the caudomedial VTA (interfascicular nucleus), with the VTA and IPN projecting to many common brain areas including the dorsal tegmental nucleus, raphé nuclei and dorsomedial nucleus of thalamus. Hence, it will be important to determine if direct cross-talk between VTA and IPN, or integration of reward-related information from these structures at downstream brain sites47, is responsible for regulating the motivational salience of nicotine and coordinating behavioral output. Our data suggest that individuals carrying risk alleles for tobacco dependence resulting in deficient α5* nAChR function are relatively insensitive to inhibitory effects of nicotine on reward pathways, consequently extending the range of nicotine doses that have net stimulatory effects on reward systems. Such a scenario is likely to be most important in the acquisition of the tobacco habit in which experiencing a negative effect of nicotine on reward pathways may decrease the likelihood of repeatedly engaging in smoking behavior64. As such, these findings have important implications for understanding the high incidence of lung cancer and COPD in individuals carrying *CHRNA5* risk alleles, suggesting that far higher levels of nicotine can be tolerated in these individuals, likely resulting in greater exposure to carcinogens contained in tobacco smoke. In summary, we have established a new framework for understanding the motivational drives that control nicotine intake. These findings are a key advance in our understanding of brain systems that regulate vulnerability to tobacco addiction, and reveal the importance of a5* nAChRs as targets for the development of novel smoking cessation therapeutics.

Methods Summary

Mice with null mutation in the α5 nAChR subunit gene and their wildtype littermates, or male Wistar rats (Charles River Laboratories, Raleigh, NC), were surgically prepared with

silastic catheters in the jugular vein and trained to respond on an “active” lever for food pellets under a fixed ratio 5 time-out 20 sec (FR5TO20) schedule of reinforcement. Mice and rats then responded for nicotine infusions on the FR5TO20 sec reinforcement schedule during 1 h daily testing sessions. Nicotine hydrogen tartrate salt was dissolved in sterile saline solution (0.9% w/v). Each nicotine reward earned resulted in the delivery of a nicotine infusion (0.033 ml injection volume delivered over 3-sec in mice; 0.1 ml delivered over 1-sec in rats) and initiated a 20-sec time-out period signaled by a light cue located above the active lever during which responding on the lever was without consequence.

Methods

Animals

Male and female mice with null mutation of the α5 nAChR subunit gene *Chrna5* (α5 knockout) and their wildtype littermates were bred in our animal facilities. Brain structure and baseline behavioral measures between the knockout mice and wildtype littermates1. The mutant mice have been bred for more than 10 generations onto a C57BL6 background. Breeding was conducted by mating heterozygous pairs. All mice were housed in cages of 1–3 and were at least 6 weeks of age at the beginning of each experiment. Male Wistar rats weighing 275–300g were purchased from Charles River Laboratories and housed 1–2 per cage. Mice and rats were maintained in an environmentally controlled vivarium on a 12h: 12h reversed light:dark cycle, and food and water were provided *ad libitum* until behavioral training commenced. During self-administration procedures, mice and rats were food restricted to 85–90% of their free-feeding body weight, but water was maintained without restriction. All procedures were conducted in strict accordance with the NIH Guide for the Care and Use of Laboratory Animals and were approved by the Institutional Animal Care and Use Committee of The Scripps Research Institute - Florida.

Genotyping

Around 21 days of age, mouse pups were weaned and their tails were clipped for genetic analysis. DNA was extracted with a tissue DNA extraction kit purchased from Biomiga, Inc. (San Diego, CA). Primers for the α5 wildtype and mutant genes were: α5 wildtype forward (5'-CACTGTCACTTGGACGCAGCC-3'); α5 wildtype reverse (5'-GTTCCCCTTGCTCCCCATTGC-3'), Neo-1 (5'-CTTTTTGTCAAGACCGACCTGTCCG-3'); and Neo-2 (5'-CTCGATGCGATGTTTCGCTTGGTG-3'). Samples were processed for genetic amplification with PCR and subsequently run on a 1% agarose gel with ethidium bromide. The band for the α5 wildtype gene was at 190bp, and the α5 mutant gene was at 290bp.

Drugs

For self-administration experiments in mice and rats, (−)-nicotine hydrogen tartrate salt (Sigma Chemical Co., St. Louis, MO) was dissolved in 0.9% sterile saline. All doses of nicotine refer to the free-base form. The NMDA antagonist LY235959 (Tocris, Ellisville, MO) or lidocaine (2%, Sigma Chemical Co.) were microinjected at a volume of 0.5 μl for over 1 min, and the injector remained in place for an additional 2 min to allow for diffusion. The pH of solutions was adjusted to ~7.4.

Surgery

Mice and rats were anesthetized with an isoflurane (1–3%)/oxygen vapor mixture and prepared with intravenous catheters. Briefly, the catheters consisted of a 6 cm (mice) or 12 cm (rats) length of silastic tubing fitted to guide cannula (Plastics One, Wallingford, CT) bent at a curved right angle and encased in dental acrylic. The catheter tubing was passed subcutaneously from the animal's back to the right jugular vein, and a 1 cm (mice) or 2.5 cm (rats) length of the catheter tip was inserted into the vein and tied with surgical silk suture. Catheters were flushed daily with physiological sterile saline solution (0.9% w/v) containing heparin (10–60 USP units/ml). Catheter integrity was tested with the ultra short-acting barbiturate anesthetic Brevital® (methohexital sodium, Eli Lilly, Indianapolis, IN).

Intravenous self-administration

Mice and rats were mildly food restricted to 85–90% of their free-feeding body weight and trained to press a lever in an operant chamber (Med Associates, St. Albans, VT) for food pellets (20 mg pellets mice; 45 mg food pellets rats; TestDiet, Richmond, IN) under a fixed-ratio 5, time out 20 sec (FR5TO20 sec) schedule of reinforcement prior to catheter implantation. Once stable responding was achieved (>30 pellets per session in mice; >90 pellets per session in rats), subjects were catheterized as described above. The animals were allowed at least 48 h to recover from surgery, then permitted to respond for food reinforcement again under the FR5TO20 sec schedule. Once food responding criteria was reestablished, subjects were permitted to acquire intravenous nicotine self-administration by autoshaping during 1 h daily sessions, 7 days per week. Nicotine was delivered through the tubing into the intravenous catheter by a Razel syringe pump (Med Associates). Each nicotine self-administration session was performed using 2 retractable levers (1 active, 1 inactive) that extend 1 cm into the chamber. Completion of the response criteria on the active lever resulted in the delivery of an intravenous nicotine infusion (0.03 ml infusion volume for mice; 0.1 ml for rats). Responses on the inactive lever were recorded but had no scheduled consequences. For dose-response studies (fixed and progressive ratio schedules), animals were presented with each dose of nicotine for at least 5 days (mice) or 3 days (rats); the mean intake over the last 3 (mice) or 2 (rats) sessions for each dose was calculated and used for statistical analysis. Nicotine doses were presented according to a within-subjects Latin square design. In between each dose, subjects were placed back on the training dose for at least 2 days or until their intake returned to baseline levels before being tested on the next dose in the Latin-square design.

Surgical procedures for microinjections and ICSS electrode placement

Animals were anesthetized as above and positioned in a stereotaxic frame (Kopf Instruments, Tujunga, CA). Unless otherwise noted, the incisor bar was set to the `flat-skull' position. To test the efficacy of the re-expressing and knockdown viruses *in vivo*, bilateral injections were made into the hippocampus of mice or rats, respectively. This area was chosen based on the constitutive expression of α5 nAChR subunit mRNA in wildtype animals. In mice, six bilateral injections (1 μl each at a flow rate of 1 μl per min) were made at the following coordinates: anterior-posterior (AP): −1.7 mm from bregma; medial-lateral (ML): ±0.75 mm from midline; dorsal-ventral (DV): −2.05 mm, −1.80 mm and −1.3 5mm

from brain surface2. In rats, the six hippocampal injections (three 2 μl injections per side at a flow rate of 1 μl per min) were made at the following coordinates: AP: −3.3 mm from bregma; ML: ±1.1 mm from midline; DV: −3.6 mm, −3.0 mm and −2.4 mm from brain surface3. For habenular injections in mice, the needle was angled 20° toward midline, and bilateral injections (0.375 μl each) were administered at a rate of 0.375 μl per min. For habenular injections in rats, the lentivirus was injected bilaterally based on previously published coordinates4. The incisor bar was set to 5 mm above plane, and the injector needle was at a 10° angle toward midline (AP: −2.2 mm from bregma; ML: ±1.5 mm from midline; DV: −4.9 mm from brain surface). The bilateral injections (1 μl each) were administered at a rate of 1 μl per min. For all of the injections, the injector needle was remained in place for a minimum of 2 min post-injection. For IPN and VTA microinjections in rats, guide cannula (Plastics One) were implanted as follows: IPN (flat skull; 10° angle toward midline; AP: −6.72 mm from bregma; ML: ±1.6 mm from midline; DV: −6.5 mm from brain surface) or VTA (bilateral; flat skull; 6° angle toward midline; AP: −5.4 mm from bregma; ML: ±1.3 mm from midline; DV: −7.0 mm from skull)3. The MHb guide cannula coordinates were the same as for the lentiviral injections, except with DV at −2.9 mm from brain surface. For all of the cannula, injector needles extended 2 mm below the tip of the cannula for placement into the brain region. For the ICSS electrode, a stainless steel bipolar electrode (Plastics One) was implanted into the lateral hypothalamus (AP: −0.5 mm from bregma; ML: ±1.7 mm from midline; DV: −8.3 mm from brain surface)3.

BSR Behavioral Procedure

Rats were trained to respond according to a modification of the discrete-trial current-threshold BSR procedure of Kornetsky and Esposito5,6 in an operant box equipped with a wheel manipulandum and ICSS stimulator (Med Associates). Briefly, a trial was initiated by the delivery of a non-contingent electrical stimulus. This electrical reinforcer had a duration of 500 ms and consist of 0.1 ms rectangular cathodal pulses that delivered at a frequency of 50–100 Hz. The frequency of the stimulation was selected for individual rats so that threshold elevation and lowering may be detected, and this frequency was held constant throughout the experiment. A one-quarter turn of the wheel manipulandum within 7.5 sec of the delivery of the non-contingent stimulation resulted in the delivery of an electrical stimulus identical in all parameters to the non-contingent stimulus that initiated the trial. After a variable inter-trial interval (7.5–12.5 sec, mean of 10 sec), another trial was initiated with the delivery of a non-contingent electrical stimulus. Failure to respond to the non-contingent stimulus within 7.5 sec resulted in the onset of the inter-trial interval. Responding during the inter-trial interval delayed the onset of the next trial by 12.5 sec. In each testing session, current levels were varied in alternating descending (x2) and ascending (x2) series in 5 μA steps. A set of five trials was presented for each current intensity. The threshold for each series is defined as the midpoint between two consecutive current intensities that yield “positive scores” (animals respond for at least three of the five trials) and two consecutive current intensities that yield “negative scores” (animals do not respond for three or more of the five trials). The overall threshold for the session is defined as the mean of the thresholds for the four individual series. Threshold data are presented as percent of baseline values due to inter-subject variability in baseline rates.

Generation of lentivirus

For α5 subunit re-expression studies, the mouse α5 nAChR subunit gene,*Chrna5*, was cloned into the pCDF1 lentivirus expression vector containing cop-GFP from Systems Biosciences, Inc. (Mountain View, CA). For α5 subunit knockdown studies, two different short hairpin interfering RNAs (shRNA) directed against the rat *Chrna5* gene were were designed using the Genscript, Inc. online construct builder (see Supplementary Figs for shRNA sequence). The shRNAs were cloned into the pRNAT-U6.2/Lenti construct containing GFP (GenScript, Piscataway, NJ). Control vectors were identical to the expression constructs, but without the gene insert.

Generation of lentivirus

To generate lentivirus supernatant, HEK-293FT packaging cells (3.75×10^6 293TN cells per 10 cm plate) were transfected with the vectors, along with the pPACKF1TM Lentiviral Packaging Kit using lipofectamine reagent and plus reagent (Invitrogen) according to the manufacturer's instructions. Medium containing virus particles (~10 ml) was harvested 48–60 h post-transfection by centrifugation at 76,755g at room temperature for 5 min to pellet cell debris and filtered through 0.45 mm PVDF filters (Millex-HV). To concentrate the viral supernatant for intrastriatal administration, supernatants were centrifuged at 32,000g for 90 min at 4 °C, and the precipitate re-suspended in 100 μl cold PBS. Supernatants were aliquoted into 10 ml volumes and stored at −80 °C until use.

Estimation of lentivirus titer

Viral supernatant titres were determined using the Lentivector Rapid Titer Kit from System Biosciences, according to the manufacturer's instructions. The number of infectious units per ml of supernatant (IFU ml^{-1}) was calculated as follows: Multiplicity of infection (MOI) of the sample × the number of cells in the well upon infection × 1,000 / μl of viral supernatant used.

Tissue dissection

Mice and rats were euthanized by inhalation of CO_2, brains were rapidly removed, and frozen on dry ice. Tissues were stored at −80°C until dissection. Brains were sliced on a cryostat, and bilateral dissections were made for the hippocampus, habenula, IPN and/or VTA with a scalpel. Samples were pooled across multiple subjects due to the small size of selected brain areas and stored in at −80°C until processing for RNA isolation.

RNA Isolation and real-time RT-PCR

Cells grown in monolayer or dissected tissue was homogenized in RNA-STAT60 (Tel-Test Inc., Friendswood, TX) using a 27 gauge needle. Following homogenization, 250 μl of chloroform was added and the samples were vortexed for 1 min. Samples were then centrifuged for 15 min at 12,000 × g at 4°C, and the upper aqueous RNA containing layer was removed for an additional RNASTAT60/chloroform extraction. The RNA was precipitated with 2 × volume of isopropanol overnight at −20°C and centrifuged for 30 min at 12000 × g. The RNA pellets were washed twice with 70% ethanol/RNAase-free water and subsequently resuspended in RNAsecure (Ambion/Applied Biosystems, Austin, TX), and

~10 μg of RNA from each sample was treated with Turbo DNase (Ambion/Applied Biosystems) for 60 min at 37°C to degrade residual genomic DNA. To assess RNA levels, samples were reverse transcribed into cDNA with the TaqMan High Capacity cDNA Reverse Transcription kit (Applied Biosystems, Foster City, CA). Thereafter, they were processed with the TaqMan Universal PCR kit with the mouse or rat *CHRNA5* gene expression assay (Applied Biosystems); controls consisted of either β-actin or 18S. Samples were quantified by real-time RT-PCR (7900 Real-Time PCR system; Applied Biosystems). All data were normalized in accordance with the mean housekeeping mRNA expressing levels as an internal control. Comparison between groups made using the method of $2^{-\Delta\Delta Ct}$.

Brain Perfusion and Fixation

Subjects were anesthetized with sodium pentobarbital (0.1 mg/10 g body weight) and perfused through the ascending aorta with 0.9% saline, followed by 4% paraformaldehyde in 0.1 M phosphate buffer solution (PBS; pH 7.4). Brains were harvested, postfixed for 2 hrs in 4% paraformaldehyde, and then stored in 30% sucrose in PBS. All brains were cut into 30–40 μm coronal sections on a microtome, and the floating sections were stored in 0.1 M PBS with 0.01% sodium azide at 4°C until processing for immunocytochemistry.

Fluorescence Immunolabeling

Floating sections were processed for GFP fluorescent immunostaining. To localize the GFP-tagged lentivirus-infected cells in mice, we utilized a rabbit polyclonal IgG that recognizes GFP cloned from copepod *Pontellina plumata* (copGFP). To localize the lentivirus tagged with GFP in rats, we utilized a chicken polyclonal IgG that recognizes a 27kDa protein derived from the jellyfish *Aequorea Victoria*. Further, to identify IPN we utilized a guinea pig polyclonal IgG that recognizes VAChT. Sections were rinsed in 0.1M PBS, pH 7.4, with 0.3% Triton-X 100 (PBT) and then blocked in 10% normal donkey serum/PBT. Thereafter, sections were incubated in the primary antibody in PBT at 4°C overnight. The primary antibodies were diluted as follows: rabbit anti-copGFP (1:2,000; Evrogen, Moscow, Russia), chicken anti-GFP (1:2,000; Millipore, Billercia, MA) or guinea pig anti-VACHT (1:500; Millipore). On day 2, the sections were rinsed and incubated in Alexa 488 donkey anti-rabbit (1:400; Invitrogen), DyLight 488 donkey anti-chicken (1:400; Jackson ImmunoResearch, West Grove, PA) and/or DyLight 594 or 647 donkey anti-guinea pig (1:500; Jackson ImmunoResearch) secondary antibodies in 0.3% PBT for 2 hrs. Next, the sections were rinsed, mounted on slides with vectashield (with or without DAPI) (Vector Labs, Burlingame, CA), and coverslipped. Controls included processing the secondary antibodies alone to verify background staining, processing each primary with the secondary antibody to verify laser-specific excitation, examining for autofluorescence in an alternate laser channel with tissue lacking that laser-specific probe, and using sequential scanning. For subsequent fluorescent images, only the brightness and/or contrast levels were adjusted post-acquisition and were imposed across the entire image.

$^{86}Rb^{+}$ Efflux

86RbCl (average initial specific activity 15 Ci/mg) as well as Optiphase Supermix scintillation cocktail was purchased from Perkin-Elmer NEN (Boston, MA). The α5

knockout mice were injected with either the Lenti-CHRNA5 or Lenti-Control vector as previously described. Following an incubation period of at least 3 weeks, mice were killed synaptosomes generated from the IPN, habenula, hippocampus, striatum, thalamus and cortex as described previously 7. Samples were loaded with $86Rb^+$ and acetylcholine-stimulated $86Rb^+$ efflux was measured as described previously7, with each sample stimulated only once. $86Rb^+$ efflux was expressed as the increase in signal above basal efflux. A non-linear least squares curve fit to a first order equation ($C_t = C_0 * e^{-kt}$), where C_t is the basal efflux counts at time, t, C_0 is the estimated efflux counts at t = 0 sec, and k is the first order decay constant) was used to estimate basal efflux for each sample. Counts in fractions preceding and following the peak were used for curve fitting. Acetylcholine-stimulated efflux was calculated by summing the counts in the fractions exceeding basal efflux during ACh exposure and dividing by the corresponding basal efflux counts. This value represents total peak relative to baseline.

Fos Procedure

Wildtype and α5 subunit knockout mice were injected subcutaneously with nicotine (0.5 or 1.5 mg/kg, free-base) or saline. The moderate dose of nicotine is known to be rewarding in these mice, reflected in the conditioning of a place preference8. The higher dose of nicotine is aversive, reflected in the induction of a conditioned taste aversion in wildtype mice9. After 2 hr, each subject was perfused and brains were removed and stored as described above. Brain sections were cut at 30μm on a cryostat and stored in 0.1M PBS with 0.01% sodium azide until processing. For Fos immunolabeling, sections were rinsed in 0.1M PBS (ph 7.4), treated with 0.3% H_2O_2-PBS for 15 min, rinsed in PBS, and then blocked in 10% normal goat serum and 0.5% Triton X-100 in PBS for 1 hr. Thereafter, sections were incubated in rabbit anti-cfos IgG (1:500 dilution; Abcam, Cambridge, MA) in 0.5% Triton-PBS overnight at 4°C. The following day, sections were incubated at room temperature for 2 hrs, rinsed in PBS, and then incubated in 1:300 dilution of goat anti-rabbit secondary IgG (Vector Labs) in 0.5% Triton X-100 in PBS for 2 hrs. Following rinsing, sections were incubated in ABC Elite (Vector Labs) for 90 min, rinsed in PBS, and immunoreactivity was revealed by using 3-diaminobenzidine (DAB) with nickel (Vector Labs). To reduce variability in the background and to standardize the staining, sections from subjects across groups were processed concurrently. Sections were mounted and coverslipped with Permount (Fisher Scientific). Cell numbers and region volumes for the interpeduncular nucleus, ventral tegmental area and ventromedial hypothalamus were quantified under 40× magnification using unbiased stereological methods and the optical fractionator probe with Stereo Investigator software (MicroBrightField, Inc., Williston, VT). This method of assessing total volume and cell number has been validated and employed in many prior studies. Total cell counts and area measurements were determined for each brain area, and cell density (number of cells per cubic millimeter) was calculated for each subject.

Statistical Analyses

All data were analyzed by one- or two-way analysis of variance (ANOVA) or t-test using Graphpad Prism software (La Jolla, CA). Significant main or interaction effects were followed by Bonferroni or Newman-Keuls post-hoc tests as appropriate. The criterion for significance was set at $p<0.05$.

Supplementary Material

Refer to Web version on PubMed Central for supplementary material.

Acknowledgements

Supported by the National Institute on Drug Abuse (DA020686 to PJK; DA026693 to CDF; P30DA015663 to MJM), and The James and Esther King Biomedical Research Program, Florida Department of Health (07KN-06 to PJK). This is manuscript #20591 from Scripps Florida.

References

1. Mokdad AH, Marks JS, Stroup DF, Gerberding JL. Actual causes of death in the United States, 2000. JAMA. 2004; 291:1238–1245. [PubMed: 15010446]
2. Stolerman IP, Jarvis MJ. The scientific case that nicotine is addictive. Psychopharmacology (Berl). 1995; 117:2–10. [PubMed: 7724697]
3. Le Novere N, Corringer PJ, Changeux JP. The diversity of subunit composition in nAChRs: evolutionary origins, physiologic and pharmacologic consequences. J Neurobiol. 2002; 53:447–456. [PubMed: 12436412]
4. Picciotto MR, et al. Acetylcholine receptors containing the beta2 subunit are involved in the reinforcing properties of nicotine. Nature. 1998; 391:173–177. [PubMed: 9428762]
5. Tapper AR, et al. Nicotine activation of alpha4* receptors: sufficient for reward, tolerance, and sensitization. Science. 2004; 306:1029–1032. [PubMed: 15528443]
6. Corrigall WA, Franklin KB, Coen KM, Clarke PB. The mesolimbic dopaminergic system is implicated in the reinforcing effects of nicotine. Psychopharmacology (Berl). 1992; 107:285–289. [PubMed: 1615127]
7. Ikemoto S, Qin M, Liu ZH. Primary reinforcing effects of nicotine are triggered from multiple regions both inside and outside the ventral tegmental area. J Neurosci. 2006; 26:723–730. [PubMed: 16421292]
8. Maskos U, et al. Nicotine reinforcement and cognition restored by targeted expression of nicotinic receptors. Nature. 2005; 436:103–107. [PubMed: 16001069]
9. Berrettini W, et al. Alpha-5/alpha-3 nicotinic receptor subunit alleles increase risk for heavy smoking. Mol Psychiatry. 2008; 13:368–373. [PubMed: 18227835]
10. Saccone SF, et al. Cholinergic nicotinic receptor genes implicated in a nicotine dependence association study targeting 348 candidate genes with 3713 SNPs. Hum Mol Genet. 2007; 16:36–49. [PubMed: 17135278]
11. Liu JZ, et al. Meta-analysis and imputation refines the association of 15q25 with smoking quantity. Nat Genet. 2010; 42:436–440. [PubMed: 20418889]
12. Bierut LJ, et al. Variants in nicotinic receptors and risk for nicotine dependence. Am J Psychiatry. 2008; 165:1163–1171. [PubMed: 18519524]
13. Kuryatov A, Berrettini W, Lindstrom J. Acetylcholine Receptor (AChR) {alpha}5 Subunit Variant Associated with Risk for Nicotine Dependence and Lung Cancer Reduces ({alpha}4{beta}2)2{alpha}5 AChR Function. Mol Pharmacol. 2011; 79:119–125. [PubMed: 20881005]
14. Hung RJ, et al. A susceptibility locus for lung cancer maps to nicotinic acetylcholine receptor subunit genes on 15q25. Nature. 2008; 452:633–637. [PubMed: 18385738]
15. Wang Y, Broderick P, Matakidou A, Eisen T, Houlston RS. Role of 5p15.33 (TERT-CLPTM1L), 6p21.33 and 15q25.1 (CHRNA5-CHRNA3) variation and lung cancer risk in never-smokers. Carcinogenesis. 2010; 31:234–238. [PubMed: 19955392]
16. Amos CI, et al. Genome-wide association scan of tag SNPs identifies a susceptibility locus for lung cancer at 15q25.1. Nat Genet. 2008; 40:616–622. [PubMed: 18385676]
17. Le Marchand L, et al. Smokers with the CHRNA lung cancer-associated variants are exposed to higher levels of nicotine equivalents and a carcinogenic tobacco-specific nitrosamine. Cancer Res. 2008; 68:9137–9140. [PubMed: 19010884]

18. Henningfield JE, Goldberg SR. Nicotine as a reinforcer in human subjects and laboratory animals. Pharmacol Biochem Behav. 1983; 19:989–992. [PubMed: 6657732]
19. Le Foll B, Wertheim C, Goldberg SR. High reinforcing efficacy of nicotine in non-human primates. PLoS ONE. 2007; 2:e230. [PubMed: 17311094]
20. Risner ME, Goldberg SR. A comparison of nicotine and cocaine self-administration in the dog: fixed-ratio and progressive-ratio schedules of intravenous drug infusion. J Pharmacol Exp Ther. 1983; 224:319–326. [PubMed: 6822957]
21. Corrigall WA, Coen KM. Nicotine maintains robust self-administration in rats on a limited-access schedule. Psychopharmacology (Berl). 1989; 99:473–478. [PubMed: 2594913]
22. Jackson KJ, et al. Role of alpha5 nicotinic acetylcholine receptors in pharmacological and behavioral effects of nicotine in mice. J Pharmacol Exp Ther. 2010; 334:137–146. [PubMed: 20400469]
23. Matta SG, et al. Guidelines on nicotine dose selection for in vivo research. Psychopharmacology (Berl). 2007; 190:269–319. [PubMed: 16896961]
24. Russell MA, Wilson C, Patel UA, Feyerabend C, Cole PV. Plasma nicotine levels after smoking cigarettes with high, medium, and low nicotine yields. Br Med J. 1975; 2:414–416. [PubMed: 1168517]
25. Lynch WJ, Carroll ME. Regulation of drug intake. Exp Clin Psychopharmacol. 2001; 9:131–143. [PubMed: 11518086]
26. Lynch WJ, Carroll ME. Regulation of intravenously self-administered nicotine in rats. Exp Clin Psychopharmacol. 1999; 7:198–207. [PubMed: 10472507]
27. Marks MJ, et al. Nicotine binding and nicotinic receptor subunit RNA after chronic nicotine treatment. J Neurosci. 1992; 12:2765–2784. [PubMed: 1613557]
28. Herkenham M, Nauta WJ. Efferent connections of the habenular nuclei in the rat. J Comp Neurol. 1979; 187:19–47. [PubMed: 226566]
29. Grady SR, et al. Rodent habenulo-interpeduncular pathway expresses a large variety of uncommon nAChR subtypes, but only the alpha3beta4* and alpha3beta3beta4* subtypes mediate acetylcholine release. J Neurosci. 2009; 29:2272–2282. [PubMed: 19228980]
30. London ED, Connolly RJ, Szikszay M, Wamsley JK, Dam M. Effects of nicotine on local cerebral glucose utilization in the rat. J Neurosci. 1988; 8:3920–3928. [PubMed: 3193185]
31. Donovick PJ, Burright RG, Zuromski E. Localization of quinine aversion within the septum, habenula, and interpeduncular nucleus of the rat. J Comp Physiol Psychol. 1970; 71:376–383. [PubMed: 5480869]
32. Salas R, Sturm R, Boulter J, De Biasi M. Nicotinic receptors in the habenulo-interpeduncular system are necessary for nicotine withdrawal in mice. J Neurosci. 2009; 29:3014–3018. [PubMed: 19279237]
33. Glick SD, Ramirez RL, Livi JM, Maisonneuve IM. 18-Methoxycoronaridine acts in the medial habenula and/or interpeduncular nucleus to decrease morphine self-administration in rats. Eur J Pharmacol. 2006; 537:94–98. [PubMed: 16626688]
34. Matsumoto M, Hikosaka O. Lateral habenula as a source of negative reward signals in dopamine neurons. Nature. 2007; 447:1111–1115. [PubMed: 17522629]
35. Brown RW, Collins AC, Lindstrom JM, Whiteaker P. Nicotinic alpha5 subunit deletion locally reduces high-affinity agonist activation without altering nicotinic receptor numbers. J Neurochem. 2007; 103:204–215. [PubMed: 17573823]
36. Kenny PJ, Markou A. Nicotine self-administration acutely activates brain reward systems and induces a long-lasting increase in reward sensitivity. Neuropsychopharmacology. 2006; 31:1203–1211. [PubMed: 16192981]
37. Schaefer GJ, Michael RP. Task-specific effects of nicotine in rats. Intracranial self-stimulation and locomotor activity. Neuropharmacology. 1986; 25:125–131. [PubMed: 3703168]
38. Kenny PJ. Brain reward systems and compulsive drug use. Trends Pharmacol Sci. 2007; 28:135–141. [PubMed: 17276521]
39. Qin C, Luo M. Neurochemical phenotypes of the afferent and efferent projections of the mouse medial habenula. Neuroscience. 2009; 161:827–837. [PubMed: 19362132]

40. Hussain RJ, Taraschenko OD, Glick SD. Effects of nicotine, methamphetamine and cocaine on extracellular levels of acetylcholine in the interpeduncular nucleus of rats. Neurosci Lett. 2008; 440:270–274. [PubMed: 18583043]
41. Girod R, Barazangi N, McGehee D, Role LW. Facilitation of glutamatergic neurotransmission by presynaptic nicotinic acetylcholine receptors. Neuropharmacology. 2000; 39:2715–2725. [PubMed: 11044742]
42. McGehee DS, Heath MJ, Gelber S, Devay P, Role LW. Nicotine enhancement of fast excitatory synaptic transmission in CNS by presynaptic receptors. Science. 1995; 269:1692–1696. [PubMed: 7569895]
43. Rauhut AS, Hawrylak M, Mardekian SK. Bupropion differentially alters the aversive, locomotor and rewarding properties of nicotine in CD-1 mice. Pharmacol Biochem Behav. 2008; 90:598–607. [PubMed: 18556053]
44. Gavrilov YV, Perekrest SV, Novikova NS, Korneva EA. Stress-induced changes in cellular responses in hypothalamic structures to administration of an antigen (lipopolysaccharide) (in terms of c-Fos protein expression). Neurosci Behav Physiol. 2008; 38:189–194. [PubMed: 18197387]
45. Laviolette SR, Alexson TO, van der Kooy D. Lesions of the tegmental pedunculopontine nucleus block the rewarding effects and reveal the aversive effects of nicotine in the ventral tegmental area. J Neurosci. 2002; 22:8653–8660. [PubMed: 12351739]
46. Kenny PJ, Chartoff E, Roberto M, Carlezon WA Jr. Markou A. NMDA receptors regulate nicotine-enhanced brain reward function and intravenous nicotine self-administration: role of the ventral tegmental area and central nucleus of the amygdala. Neuropsychopharmacology. 2009; 34:266–281. [PubMed: 18418357]
47. Hong LE, et al. A genetically modulated, intrinsic cingulate circuit supports human nicotine addiction. Proc Natl Acad Sci USA. 2010; 107:13509–13514. [PubMed: 20643934]

References

1. Salas R, et al. The nicotinic acetylcholine receptor subunit alpha 5 mediates short-term effects of nicotine in vivo. Mol Pharmacol. 2003; 63:1059–1066. [PubMed: 12695534]
2. Paxinos, G.; Franklin, KBJ. The mouse brain in stereotaxic coordinates. Second Edition edn. Academic Press; 2001.
3. Paxinos, G.; Watson, C. The rat brain in stereotaxic coordinates. Third Edition edn. Academic Press; 1997.
4. Lecourtier L, Neijt HC, Kelly PH. Habenula lesions cause impaired cognitive performance in rats: implications for schizophrenia. Eur J Neurosci. 2004; 19:2551–2560. [PubMed: 15128408]
5. Kornetsky C, Esposito RU, McLean S, Jacobson JO. Intracranial self-stimulation thresholds: a model for the hedonic effects of drugs of abuse. Arch Gen Psychiatry. 1979; 36:289–292. [PubMed: 420547]
6. Huston-Lyons D, Kornetsky C. Effects of nicotine on the threshold for rewarding brain stimulation in rats. Pharmacol Biochem Behav. 1992; 41:755–759. [PubMed: 1594644]
7. Marks MJ, et al. Two pharmacologically distinct components of nicotinic receptor-mediated rubidium efflux in mouse brain require the beta2 subunit. J Pharmacol Exp Ther. 1999; 289:1090–1103. [PubMed: 10215692]
8. Jackson KJ, et al. Role of alpha5 nicotinic acetylcholine receptors in pharmacological and behavioral effects of nicotine in mice. J Pharmacol Exp Ther. 2010; 334:137–146. [PubMed: 20400469]
9. Shoaib M, et al. The role of nicotinic receptor beta-2 subunits in nicotine discrimination and conditioned taste aversion. Neuropharmacology. 2002; 42:530–539. [PubMed: 11955523]

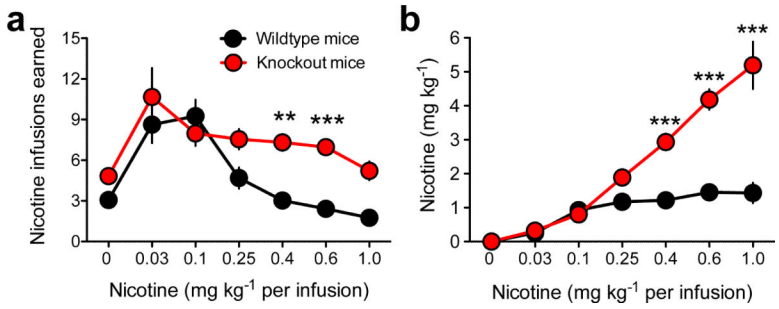

Figure 1. Increased nicotine intake in α5 subunit knockout mice

(a) Data are presented as mean (± SEM) number of nicotine infusions earned across a range of nicotine doses. Two-way ANOVA: *Genotype* $F_{(1,91)}$=28.57, p<0.0001; *Dose* $F_{(6,91)}$=13.69, p<0.0001; *Interaction* $F_{(6,75)}$=2.55, p<0.05; *n*=10–11 per group. **(b)** Data from [a] are presented as mean (± SEM) total nicotine intake at each dose. *Genotype* $F_{(1,91)}$=67.98, p<0.0001; *Dose* $F_{(6,91)}$=39.06, p<0.0001; *Interaction* $F_{(6,791}$=14.25, p<0.0001.

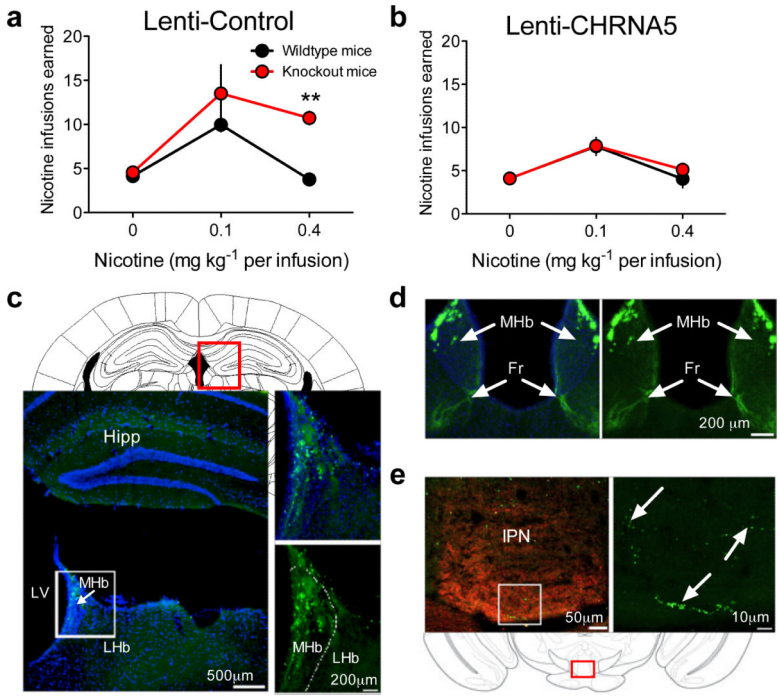

Figure 2. "Rescue" of α5* nAChRs in MHb-IPN normalizes nicotine intake

(a) Mean (± SEM) nicotine infusions in Lenti-Control mice. *Genotype* $F_{(1,22)}$=7.70, p<0.05; *Dose* $F_{(2,22)}$=19.34, p<0.0001; *Interaction* $F_{(2,22)}$=3.75, p<0.05. **P<0.01 between genotypes **(b)** (± SEM) nicotine infusions in Lenti-CHRNA5 mice. *Genotype* $F_{(1.28)}$=0.17, not significant (n.s.); *Dose* $F_{(2,28)}$=16.05, p<0.0001; *Interaction* $F_{(2,28)}$=0.36, n.s.; *n*=6–9 per group. **(c)** GFP Immunostaining confirmed MHB virus delivery. Hipp, hippocampus; LHB, lateral habenula; LV lateral ventricle; MHb, medial habenula. **(d)** GFP-labeled cells in MHb, DAPI-counterstained in left panel, extend into the fasciculus retroflexus (Fr). **(e)** GFP-positive axons detected in IPN. Left panel is labeled with VAChT (red) to identify IPN.

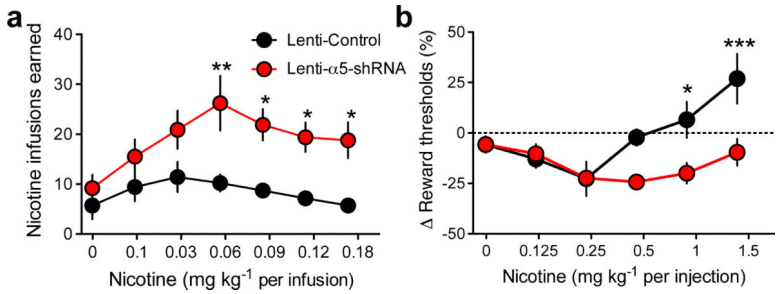

Figure 3. α5* nAChRs in MHb-IPN tract control nicotine intake and its reward-inhibiting effects in rats

(a) Nicotine self-administration in rats injected with Lenti-Control or Lenti-α5-shRNA in the MHb. Data are presented as mean (± SEM) number of nicotine infusions earned. *Lentivirus* $F_{(1,60)}$=21.07, p<0.01; *Dose* $F_{(6,60)}$=3.84, p<0.01; *Interaction* $F_{(6,60)}$=1.57, n.s.;; *n*=5–7 per group. **(b)** ICSS self-stimulation thresholds in rats. Data are presented as mean (± SEM) percentage change from baseline reward threshold. *Lentivirus* $F_{(1,60)}$=13.23, p<0.001; *Dose* $F_{(5,60)}$=6.38, p<0.0001; *Interaction* $F_{(5,60)}$=4.19, p<0.01. *p<0.05, **p<0.01 and ***p<0.001 indicates statistically significant difference between groups; *n*=6–8 per group.

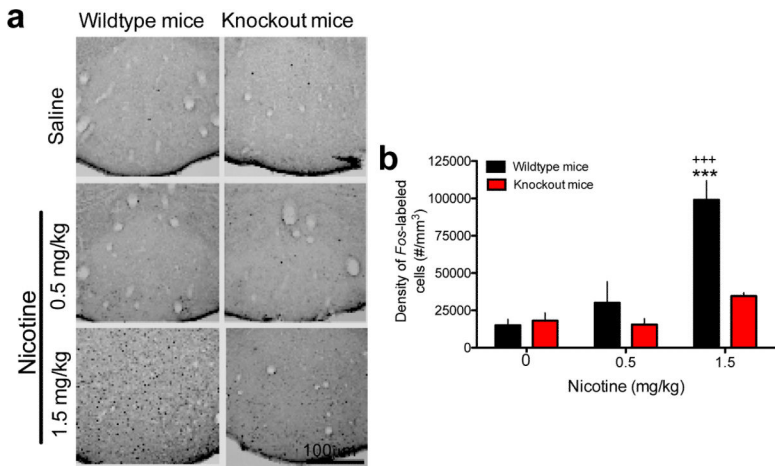

Figure 4. Nicotine-induced activation of IPN in mice

(a) Photomicrograph of IPN showing Fos immunoreactivity in wildtype (left panels) and α5 knockout (right panels) mice following saline (top panels), 0.5 mg kg^{-1} nicotine (center panels), or 1.5 mg kg^{-1} nicotine (bottom panels); *n*=5 per group. **(b)** Cell density was quantified with unbiased stereology. Data are presented as the mean (± SEM) density of Fos-immunoreactive cells (number per mm^3). *Genotype* $F_{(1,24)}$=13.50, p<0.01; *Drug* $F_{(2,24)}$=21.13, p<0.0001; *Interaction* $F_{(2,24)}$=8.64, p<0.01.

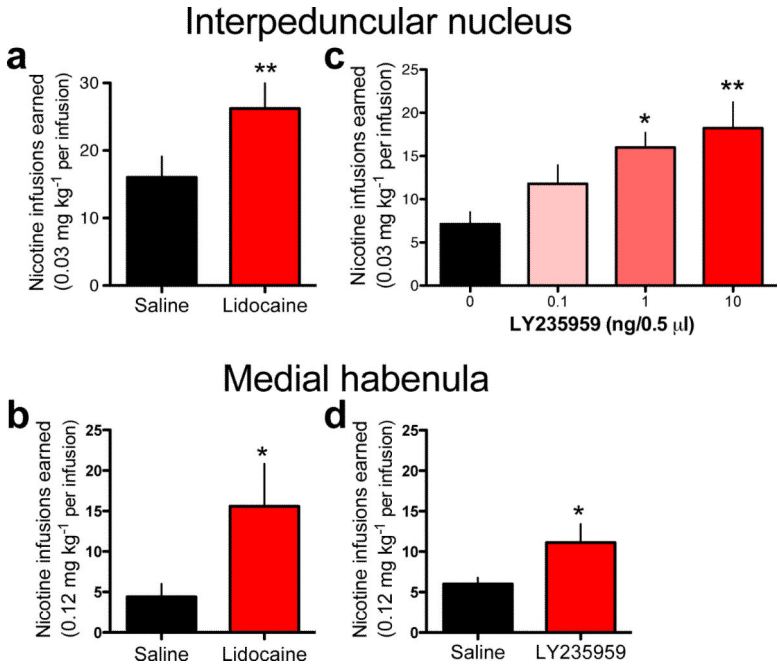

Figure 5. Disruption of IPN or MHb signaling increases nicotine intake in rats

All data are presented as mean (± SEM) number of nicotine infusions earned. **(a)** Lidocaine infused into IPN increased nicotine intake in rats; **P<0.01. **(b)** Lidocaine into MHb increased nicotine intake in rats self-administering a high unit dose (0.12 mg kg^{-1} per infusion); *P<0.05. **(c)** LY235959 infused into IPN increased nicotine intake in rats (*n*=9). $F_{(3,24)}$=6.08, p<0.01. *P<0.05 and **p<0.01 compared to control. **(d)** LY235959 (10 ng/side) into MHb increased nicotine intake in rats responding for a high unit dose (0.12 mg kg^{-1} per infusion; n=5); *P<0.05.